ACI MATERIALS JOURNAL TECHNICAL PAPER

Title no. 92-M15

# Mechanical Properties of Three High-Strength Concretes Containing Silica Fume

by J. Xie, A. E. Elwi, and J. G. MacGregor

*Three high-strength concretes containing silica fume were cast and tested at the University of Alberta to study the mechanical properties. The concretes were designed to have compressive cylinder strengths of 60, 90, and 120 MPa. The tests carried out included the compressive cylinder, split-cylinder, notched-beam, and triaxial compression tests. The objective was to determine the compressive cylinder strength, split-cylinder tensile strength, tensile fracture energy, and maximum and residual triaxial strengths. Based on the test results, some observations were made on the concrete behavior in uniaxial compression, tension, and triaxial compression. The relationship between the confinement and the maximum and residual strengths of concrete in triaxial compression was studied. The test results have been used to establish expressions of maximum and residual strengths in a finite element constitutive model for high-strength concrete.*

**Keywords:** compressive strength; confined concrete; ductility; **high-strength concretes;** residual stress; **silica fume;** triaxial stresses.

For the past two decades, high-strength concrete has demonstrated its superior performance in engineering applications. With the development of concrete technology, concrete strength of up to 100 MPa and higher can be reached without difficulties. It has been noted that high-strength concrete will play an increasingly important role in future applications.

High-strength concrete, according to the recent CEB/FIP report,[1] is defined as: "All concrete with a compressive cylinder strength above the present existing limits in national codes, i.e., about 60 MPa, and up to 130 MPa, the practical upper limit for concretes with ordinary aggregates."

In this paper, the mechanical properties of high-strength concrete are investigated in a series of tests designed to look at three aspects of behavior: 1) concrete in uniaxial compression; 2) concrete in tension (including splitting tensile tests and tests on notched beams); and 3) concrete in triaxial compression. This was done for concretes having nominal compression strengths of 60, 90, and 120 MPa at 28 days. All the tests on one strength of concrete were on specimens from the same batch of concrete. Based on these tests, envelopes of the maximum and residual strengths are proposed for triaxially loaded concrete.

## RESEARCH SIGNIFICANCE

High-strength concrete is a new structural material on which a full-fledged investigation of mechanical properties is necessary. A knowledge of high-strength concrete behavior in triaxial compression is needed to allow examination of the design rules of tied and spiral columns and other confined structures. In addition, experimental results of concrete under uniaxial and triaxial compression form an essential part in establishing a finite element constitutive model for concrete.

## PREVIOUS RESEARCH

The mechanical properties of concrete include its behavior in tension, and uniaxial and triaxial compression. In the past decade, extensive attention was placed on the strain-softening behavior of concrete in both tension and compression. There are two alternative approaches to determine the tensile fracture energy of concrete: the direct tension test[2-4] and the notched-beam test.[5,6] Previous work on triaxial compression includes the classical test series by Richart, Brandtzaeg, and Brown,[7] the test series of low-strength concrete ($f_c'$ = 32 MPa) by Palaniswamy and Shah,[8] the test series of low-strength concrete ($f_c'$ = 22.1 MPa) by Willam, Hurlbut, and Sture,[4] and the test series of low-, medium, and high-strength concrete ($f_c'$ = 25, 60, and 80 MPa) by Jensen and Bjerkeli.[9]

## DESIGN OF CONCRETE MIXES

Three batches of high-strength concrete were cast with the target compressive cylinder strengths of 60, 90, and 120 MPa (8700, 13,050, and 17,400 psi) after 28 days of curing. The mix designs for these three batches (labeled Types A, B, and C) are listed in Table 1. The materials used made a 0.085 $m^3$ (3 $ft^3$) batch of fresh concrete for each type.

The concrete contained gravel aggregate with a maximum size of 14 mm (0.55 in.). The petrographic analysis of the coarse aggregate indicated that the fraction retained on a 2.5-mm sieve is primarily composed of orthoquartzite (62.3

*ACI Materials Journal*, V. 92, No. 2, March-April 1995.
Received August 16, 1993, and reviewed under Institute publication policies.  Pertinent discussion will be published in the January-February 1996 *ACI Materials Journal* if received by October 1, 1995.

*J. Xie* is a PhD candidate at the University of Alberta, Edmonton, Alberta, Canada. His current research is on the behavior of the confinement effects on tied columns made with high-performance concrete.

ACI member **A. E. Elwi** is Professor of Civil Engineering at the University of Alberta. His research interests include nonlinear numerical analysis of reinforced concrete structures.

ACI member **James G. MacGregor** is University Professor Emeritus at the University of Alberta. He is a past president of the Institute, and is a member of ACI Committees 318, Standard Building Code; and joint ACI-ASCE Committees 441, Reinforced Concrete Columns; and 445, Shear and Torsion.

**Table 1—Mix design of high strength concrete**

| Type | A | B | C |
|---|---|---|---|
| Target compressive strength at 28 days | 60 MPa | 90 MPa | 120 MPa |
| $H_2O$ (water) | 107.2 N | 110.8 N | 97.0 N |
| Cement | 333.7 N | 391.6 N | 449.4 N |
| *w/c* | 0.321 | 0.283 | 0.216 |
| Gravel | 918.0 N | 872.2 N | 916.7 N |
| Sand | 633.2 N | 449.4 N | 462.8 N |
| Silica fume | 40.0 N | 43.6 N | 49.8 N |
| Superplasticizer | 820.0 ml | 1340.0 ml | 1540.0 ml |
| Compressive strength achieved (days) | 60.2 MPa (29) | 92.2 MPa (35) | 119.0 MPa (39) |

**Table 2—Specimen geometry and test results in uniaxial compression**

| | Specimen | Diameter *D*, mm | Height *H*, mm | Maximum stress, MPa | Average, MPa |
|---|---|---|---|---|---|
| A* | A1 | 99.5 | 199.5 | 59.61 | 60.20 |
| | A2 | 100.0 | 201.0 | 60.58 | |
| | A3 | 100.5 | 203.0 | 60.42 | |
| B* | B1 | 104.0 | 200.0 | 90.42 | 92.21 |
| | B2 | 99.0 | 200.0 | 93.17 | |
| | B3 | 100.0 | 196.0 | 93.03 | |
| C* | C1 | 100.0 | 200.0 | 120.6 | 119.0 |
| | C2 | 99.0 | 201.0 | 116.6 | |
| | C3 | 99.0 | 204.0 | 119.8 | |

*Series A was 29 days old at the time of testing, Series B was 35 days old, and Series C was 39 days old.

percent), quartzite (14.0 percent), and hard sandstone (10.5 percent). The results of the petrographic analysis of the fine aggregate indicated that it was composed primarily of hard quartz rock types such as orthoquartzite (18.9 percent), quartzite (54.9 percent), hard sandstone (4.3 percent), and chert (4.9 percent). The fineness modulus for the fine aggregate was 2.55.

The cement was Type I. The water-cement ratios (*w/c*) were in the range of 0.22 to 0.32. To achieve this low *w/c* and maintain adequate workability, it was necessary to use a lignin sulfonate superplasticizer as a water-reducing admixture. In addition, silica fume was used in all three types of concrete. The amount of silica fume used increased as the target compressive strength increased.

## BEHAVIOR IN UNIAXIAL COMPRESSION

The specimens for the uniaxial compressive cylinder tests were nominally 100 mm in diameter and 200 mm in height

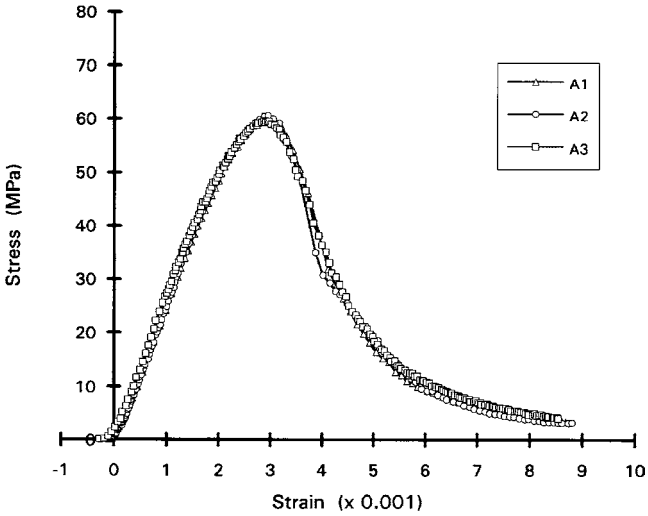


*Fig. 1—Stress-strain aspens of uniaxial compression tests (Type A concrete).*

cast in reusable plastic molds. Three specimens were tested for each type of concrete. The tests were conducted in a 2700-kN (600-kip) MTS rock testing machine. The machine had an axial stiffness of 2440 kN/mm. The tests were carried out under modified stroke control. This was done to make it possible to follow the descending branch of the stress-strain curve.

The ends of the cylinders were ground to a flat surface using a lathe and a carborundum tool. No additional sulfur cap was added. The strains were determined from the overall change of length of the specimen. This was obtained from the machine stroke corrected by

$$\text{stroke error} = \frac{P}{4000} + 0.3174(1 - e^{-P/205}),\ \text{mm} \qquad (1)$$

where $P$ (kN) is the load acting on the specimen, and $e$ is the base of natural logarithms. The geometry of specimens and test results are listed in Table 2. The stress-strain curves for concrete are presented in Fig. 1 through 3 for concrete types A, B, and C, respectively.

The strengths and the stress-strain curves for the three samples of each type of concrete were very consistent. The descending part of the stress-strain curve becomes steeper as the concrete strength increases. This suggests that high-strength concrete could be penalized by its poor ductility. It can also be noted that when the compressive strength increases, the stress-strain response in the descending part becomes more dynamic. This could be due to the difference in the failure mode of each type of concrete. For Type A concrete, since the rigidity of concrete was considerably less than the radial rigidity of the loading platens, the platens provided a considerable lateral restraint to the ends of a specimen. A cone was formed at the ends of the specimen at collapse, as shown in Fig. 4. For Types B and C concrete, the cone was only partially formed due to less confinement on its ends. Vertical cracks extended to the ends of the specimens of Types B and C concrete and eventually became major cracks that resulted in major splitting of these specimens into longitudinal pieces up to the ends at and after peak loading

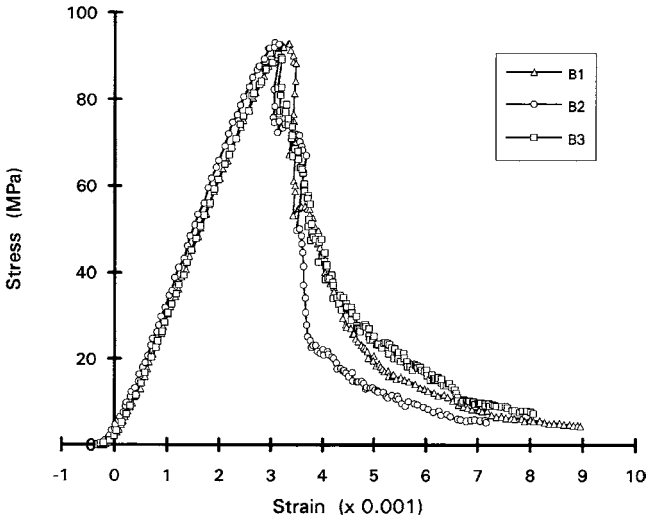


*Fig. 2—Stress-strain response of uniaxial compression tests (Type B concrete)*

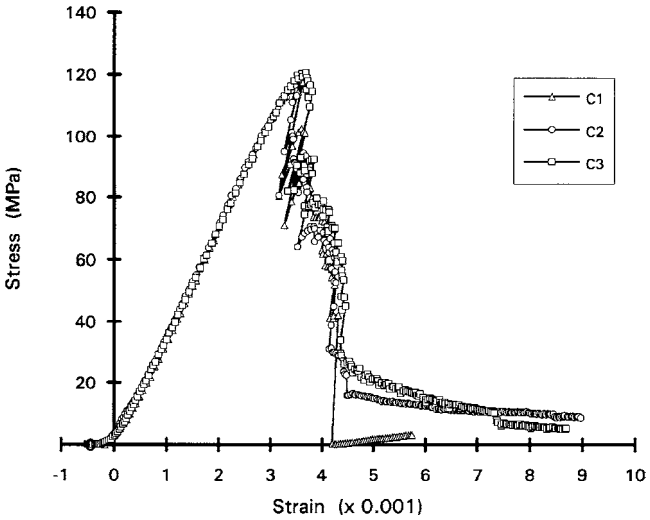


*Fig. 3—Stress-strain response of uniaxial compression tests (Type C concrete).*

(as shown in Fig. 5 for Type C concrete). The jagged descending branches of the stress-strain curves in Fig. 2 and 3 resulted from this major splitting. The load dropped on the formation of splitting, then built up again until more splitting occurred or parts of the cylinder crushed.

## BEHAVIOR IN TENSION

There are two important parameters for concrete in tension: the tensile strength and the fracture energy that reflects how concrete behaves in strain softening. In this study, the tensile strength was measured using split-cylinder tests, and the fracture energy was determined using notched-beam tests.

### Tensile strength

In this part of the investigation, three samples of each type of concrete were tested using the split-cylinder method in accordance with ASTM C 330. The specimens had a diameter $D$ = 153 mm and a length $L$ = 300 mm, and were made in reusable plastic molds. The split-cylinder tests were conducted on a Tate-Emery testing machine. The actual geometry and the test results for the three types of concrete are listed in Table 3.

The split-cylinder tensile strength $f_{ct}$ was calculated by

$$f_{ct} = \frac{2P}{\pi 2LD} \quad (2)$$

in which $P$ is the maximum splitting load recorded by the machine.

Table 3 shows that the split-cylinder tensile strength increases as the uniaxial compressive strength of the concrete increases. As expected, the increase is not directly proportional to the cylinder compressive strength.

For normal weight concrete, Carrasquillo, Nilson, and Slate[10] recommended the following relationship between the split-cylinder strength and the cylinder uniaxial compressive strength

$$f_{ct} = 0.54\sqrt{f'_c} \quad (3)$$

In this investigation, the constant in Eq. (3) appears to have higher values in the range of 0.63 to 0.68. However, the


*Fig. 4—Failure mode of uniaxial compression tests (Type A concrete).*


*Fig. 5—Failure mode of uniaxial compression tests (Type C concrete.*

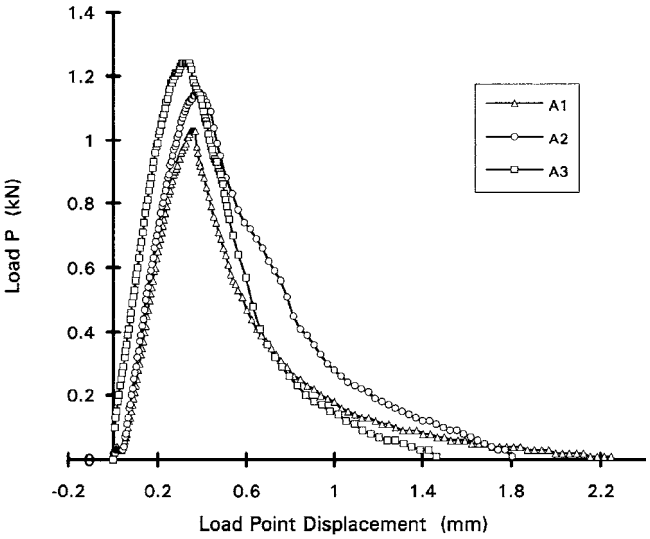


*Fig. 6—Load versus load-point displacement for notched-beam tests (Type A concrete).*

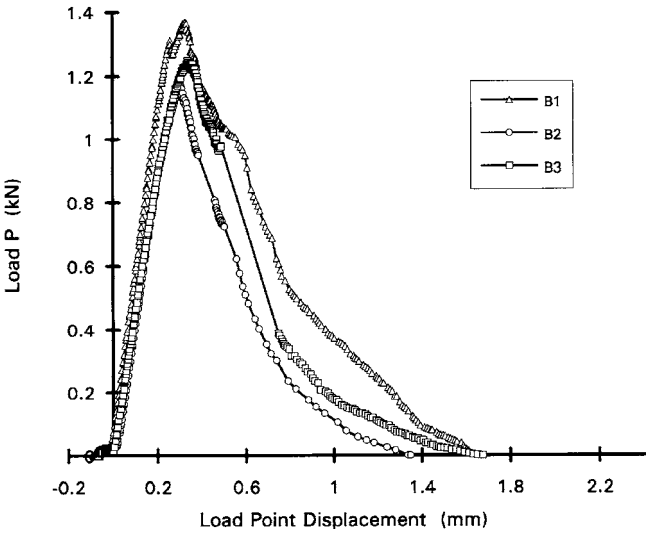


*Fig. 7—Load versus load-point displacement for notched-beam tests (Type B concrete).*

number of samples for both types of test is not sufficient to draw a general conclusion.

### Strain softening in tension

There are two alternative test approaches to quantify the strain softening of concrete in tension—the direct tension test and flexural tests on notched beams. Both types of test must be conducted under stroke control to capture the descending part of the load-deflection curve. Both types of test can be used to determine the fracture energy, an important mechanical property for concrete in tensile strain-softening.[11]

In this study, three notched beams for each type of concrete were tested to determine the tensile fracture energy. The load was applied through a steel platen that moved at a constant rate until the beam broke into two parts. The movement of the steel platen was recorded as the load-point displacement. A load cell attached to the steel platen was used to measure the magnitude of the force applied. The test specimen and procedure were in accordance with RILEM Draft Recommendation 50-FMC.[12]

**Table 3—Specimen geometry and test results in splitting test**

| Type | Specimen | Diameter *D*, mm | Length *L*, mm | Maximum *P*, kN | $f_{ct}$, MPa | Average $f_{ct}$, MPa |
|---|---|---|---|---|---|---|
| A* | A1 | 153.0 | 299.0 | 330.0 | 4.59 | 4.95 |
| | A2 | 153.0 | 300.0 | 367.0 | 4.99 | |
| | A3 | 153.0 | 301.0 | 380.0 | 5.25 | |
| B* | B1 | 153.0 | 302.0 | 480.0 | 6.61 | 6.36 |
| | B2 | 153.0 | 302.0 | 460.0 | 6.34 | |
| | B3 | 153.0 | 302.0 | 445.0 | 6.13 | |
| C* | C1 | 153.0 | 302.0 | 530.0 | 7.30 | 7.44 |
| | C2 | 153.0 | 302.0 | 510.0 | 7.03 | |
| | C3 | 153.0 | 302.0 | 580.0 | 7.99 | |

*Series A was 29 days old at the time of testing, Series B was 35 days old, and Series C was 39 days old.

The test results of load-versus-load-point displacement are presented in Fig. 6 through 8 for concrete types A, B, and C, respectively. The dimensions and test results are given in Table 4.

The tensile fracture energy, according to Peterson,[6] was calculated by

$$G_{cr}^{I} = \frac{\int_0^{\delta_{max}} P(\delta)d\delta + mg\frac{\delta_{max}}{2}}{(d-h)b} \quad (4)$$

in which $\delta$ is the load-point displacement, $\delta_{max}$ is the rupture load-point displacement, $P(\delta)$ is the load applied, $mg$ is the self-weight of the notched beam, $d$ and $b$ are the height and the width of the cross section, and $h$ is the height of the notch.

It should be mentioned that an error was made in sawing the notch in Specimen A2. Also Specimen C1 was tested under some misalignment of the load point. Excluding these two samples, average values of the fracture energy were obtained, as shown in the last column of Table 4.

The data in Table 4 suggest that the tensile fracture energy increases with increasing compressive strength. The increase is again not directly proportional to the compressive cylinder strength. As shown in Fig. 6 through 8, the post-peak part of the load-displacement response becomes steeper as the concrete compressive strength increases. This indicates that the notched beam is more brittle for higher strength concrete.

## BEHAVIOR UNDER TRIAXIAL COMPRESSION

In this study, triaxial compression tests were conducted on 11 specimens under different confinement levels for each of three types of high-strength concrete described in the previous section.

### Testing apparatus and test procedure

The triaxial compression experiments were performed in a modified Hoek rock mechanics triaxial cell, which accepts an NX core-size specimen 110 mm in height by 55.5 mm in diameter. The Hoek cell, shown in Fig. 9, can apply an axisymmetric confining pressure varying from zero to 70

**Table 4—Specimen geometry and test results for the notched beam test**

| Type | Specimen | $d$ x $b$ x $L$, mm | $h$, mm | $mg$, kN | $\sigma_{max}$, mm | $\int P(\delta)d\delta$ | $G_{cr}^{I}$, N/mm | Average $G_{cr}^{I}$, N/mm |
|---|---|---|---|---|---|---|---|---|
| | A1 | 102 x 102 x 800 | 50 | 0.209 | 2.24 | 0.563 | 0.150 | |
| A* | A2† | 102 x 102 x 750 | 51 | 0.206 | 1.85 | 0.860 | 0.202 | 0.152§ |
| | A3 | 102 x 102 x 800 | 50 | 0.206 | 1.50 | 0.663 | 0.154 | |
| | B1 | 102 x 103 x 800 | 52 | 0.214 | 1.68 | 0.701 | 0.171 | |
| B* | B2 | 100 x 103 x 780 | 50 | 0.207 | 1.32 | 0.556 | 0.135 | 0.172 |
| | B3 | 102 x 104 x 800 | 52 | 0.211 | 1.60 | 0.921 | 0.209 | |
| | C1‡ | 102 x 103 x 800 | 51 | 0.211 | 1.36 | 0.485 | 0.120 | |
| C* | C2 | 100 x 103 x 800 | 51 | 0.207 | 1.68 | 0.754 | 0.184 | 0.191‖ |
| | C3 | 101 x 103 x 800 | 50 | 0.214 | 1.54 | 0.885 | 0.199 | |

*Series A was 29 days old at the time of testing, Series B was 35 days old and Series C was 39 days old.
†Error in sawing notch.
‡Load point misaligned.
§Average $G_{cr}^{I}$ does not include the result of Specimen A2.
‖Average $G_{cr}^{I}$ does not include the result of Specimen C1.

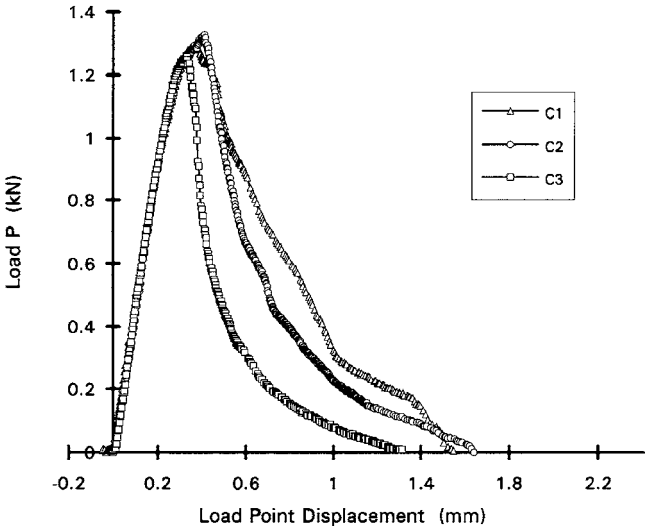


*Fig. 8—Load versus load-point-displacement for notched-beam tests (Type C concrete).*

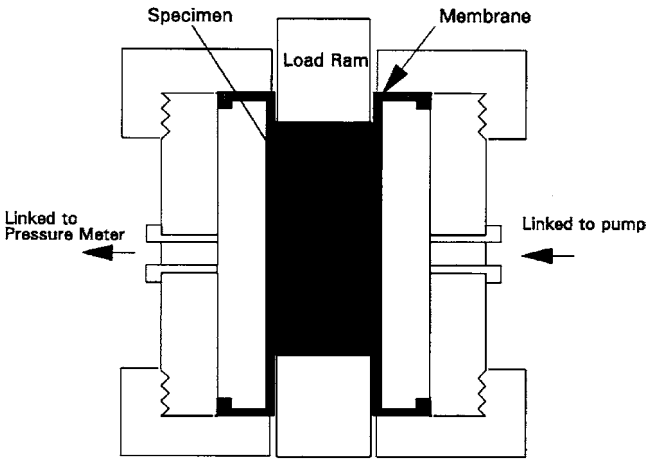


*Fig. 9—Cross-sectional view of triaxial Hoek cell.*

MPa, which was generated by a manually operated pressure supply. A flexible polyurethane membrane is used to isolate the specimen from the pressurized fluid. The membrane is not attached to the specimen or the loading ram, but, rather, is held in place by fluid pressure acting on the membrane flanges and reacting on the Hoek cell end caps.

Axial displacements were transmitted to the specimen by a steel loading ram and an MTS servo-controlled loading frame. No friction reduction was applied at the interface between the steel loading ram and the concrete specimen, thereby introducing a radial-restraint boundary condition at the specimen ends, as is typical in cylinder tests.

The concrete specimens were cast by placing the concrete into the membrane with its base sealed. The ends of specimens were ground to a flat surface in a lathe, so that full contact between the steel loading platens and the ends of the specimen was insured. To reduce the pressure sensitivity to radial displacements, only load histories with constant pressure were performed. The axial load was applied after the response due to the confinement became stable.

Eleven different confinement levels were applied in each test series with the highest held to about 50 percent of the uniaxial compressive cylinder strength for each type of concrete. Confinement ratios are shown in Table 5 for all specimens. Some of the cylinders tested with zero confinement were in air. Others had the membrane in place. The presence of the membrane provided a small degree of confinement that increased the uniaxial compressive strength by about 10 percent relative to that of those tested in air.

## Test results and discussion

The longitudinal stress-versus-average longitudinal strain results from all triaxial compressive tests are shown in Fig. 10 through 12 corresponding to concrete types A, B, and C respectively. Some qualitative observations can be made based on the test results:

*Maximum strength*—The longitudinal stress increases with increasing strain from the beginning up to a peak and then drops. The peak stress level is related to the confine-

**Table 5—Results of triaxial compression tests**

| Type (curing days) | Specimen | Confinement ratio $\sigma_1/f_c'$ | Maximum strength ratio $(\sigma_3/f_c')_{max}$ | Residual strength ratio $(\sigma_3/f_c')_{res}$ |
|---|---|---|---|---|
| A (29 days) $f_c'$ = 60.2 MPa $f_{ct}$ = 4.95 MPa | A1 | 0.038 | 1.339 | 0.703 |
| | A2 | 0.088 | 1.621 | 0.977 |
| | A3 | 0.138 | 1.788 | 1.299 |
| | A4 | 0.000 | 1.135 | 0.000 |
| | A5 | 0.337 | 2.606 | 2.344 |
| | A6 | 0.487 | 3.210 | 2.950 |
| | A7 | 0.387 | 2.858 | 2.550 |
| | A8 | 0.188 | 2.020 | 1.585 |
| | A9 | 0.238 | 2.273 | 1.859 |
| | A10 | 0.014 | 0.970 | 0.483 |
| | A11* | 0.000 | 1.070 | 0.000 |
| B (35 days) $f_c'$ = 92.2 MPa $f_{ct}$ = 6.36 MPa | B1 | 0.041 | 1.403 | 0.657 |
| | B2 | 0.090 | 1.688 | 0.932 |
| | B3 | 0.139 | 1.965 | 1.205 |
| | B4 | 0.188 | 2.107 | 1.627 |
| | B5 | 0.237 | 2.264 | 1.822 |
| | B6 | 0.285 | 2.545 | 2.037 |
| | B7 | 0.179 | 2.167 | 1.486 |
| | B8 | 0.385 | 2.832 | 2.450 |
| | B9 | 0.482 | 3.183 | 2.850 |
| | B10 | 0.000 | 1.047 | 0.000 |
| | B11* | 0.000 | 0.942 | 0.000 |
| C (39 days) $f_c'$ = 119 MPa $f_{ct}$ = 7.44 MPa | C1 | 0.051 | 1.448 | 0.630 |
| | C2 | 0.101 | 1.783 | 0.956 |
| | C3 | 0.151 | 1.898 | 1.203 |
| | C4 | 0.202 | 2.109 | 1.456 |
| | C5 | 0.252 | 2.200 | 1.645 |
| | C6 | 0.303 | 2.361 | 1.923 |
| | C7 | 0.403 | 2.658 | 2.402 |
| | C8 | 0.504 | 3.087 | 2.780 |
| | C9* | 0.000 | 0.821 | 0.000 |
| | C10 | 0.000 | 0.826 | 0.000 |
| | C11 | 0.000 | 0.965 | 0.000 |

*Specimens were tested in air.

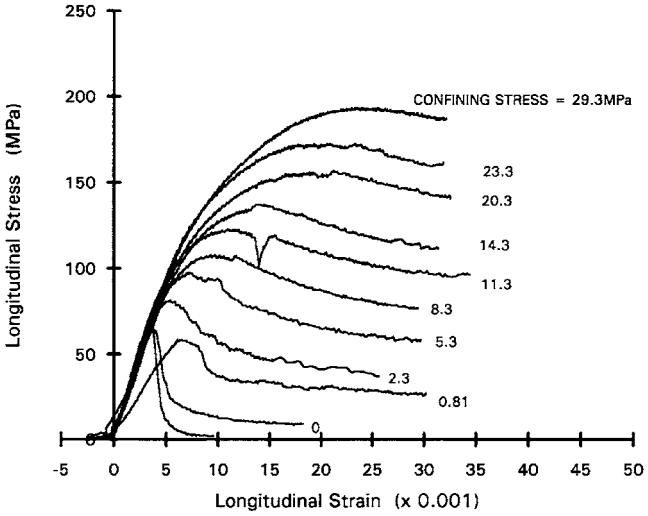


*Fig. 10—Longitudinal stress versus longitudinal strain for triaxial compression tests (Type A concrete).*

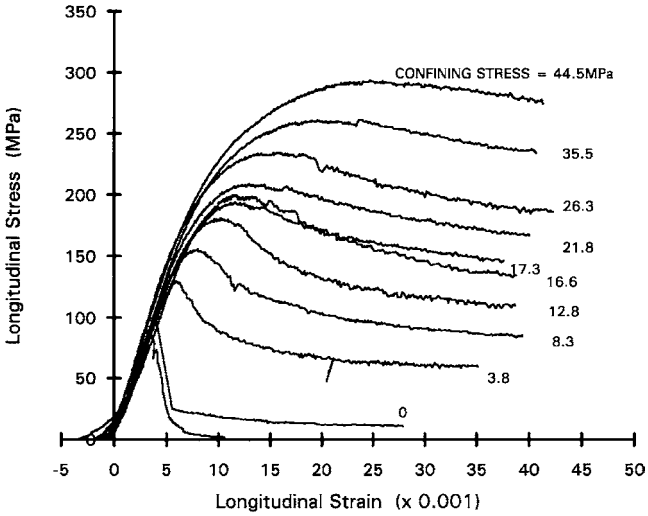


*Fig. 11—Longitudinal stress versus longitudinal strain for triaxial compression tests (Type B concrete).*

ment level. The higher the confinement, the higher the maximum strength the concrete can reach.

*Residual strength*—In the descending part of the stress-strain curve, the rate of stress decrease becomes slower with increasing longitudinal strain. Eventually, the stress tends to a constant stable level called the residual strength. This residual strength is a function of the confinement. Usually, higher confinement gives a higher residual strength.

*Ductility*—The strain corresponding to the maximum strength increases for higher confinement. On the other hand, the slope of the descending curve immediately after the peak point becomes smaller with increasing confinement. It can then be concluded that confinement greatly improves the ductility. On the other hand, increasing the uniaxial compressive strength results in poorer ductility.

*Failure modes*—For concrete with no confinement or confinement less than 15 percent of the failure mode, this consists primarily of longitudinal tensile splitting. In Type A concrete, axisymmetric cones were formed at the exterior contact with the loading platens. For concrete with high confinement, the failure mode was highly distributed with little localized damage. This allowed the stress-strain curve to vary smoothly for concrete under higher confinement.

The test results of the maximum strength and residual strength are listed in Table 5. The maximum strength was calculated from the maximum load capacity recorded by the MTS machine in the test. The residual strength was determined as the point on the descending branch of the stress-strain curve where the slope of the remaining part of the descending curve is less than 2 percent of the slope of the initial rising part of the stress-strain curve. This approach is different from that used by Willam, Hurlbut, and Sture.[4] Although not explicitly indicated in Hurlbut's report,[13] the residual strength reported there appears to be the strength when the displacement reaches the equivalent of 700 percent of the displacement at the peak loading. Since the maximum strain reached in his test was $20 \times 10^{-3}$, Hurlbut concluded that there is no strain-softening for triaxial compression specimens (with $f_c'$ = 22.1 MPa) with confinement greater

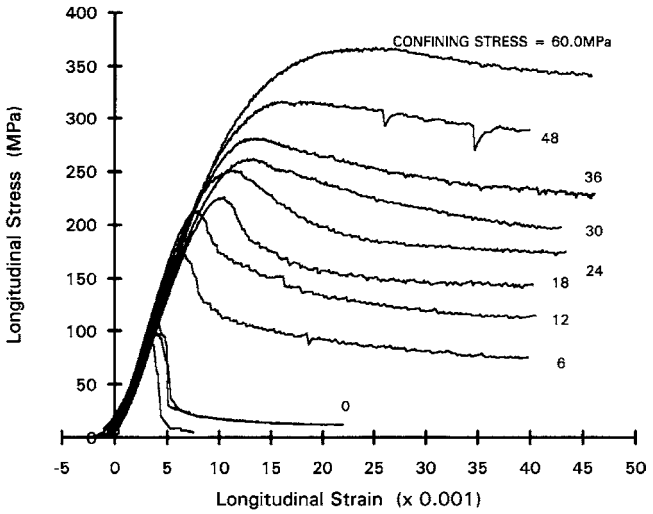


*Fig. 12—Longitudinal stress versus longitudinal strain for triaxial compression tests (Type C concrete).*

than 3.45 MPa (15.6 percent of $f_c'$). Fig. 10, 11, and 12 indicate that even when the confinement ratio is 50 percent of $f_c'$, the stress level still drops slightly after the peak stress for the concrete tested.

### Empirical equations for triaxial compressive strength

In the design of triaxially compressed structures, it is important to have equations relating the maximum strength and the confinement stress. Such equations can be established using linear or nonlinear regression analysis. In this report, *R*-square values were computed after the regression analysis to indicate how well a calculated regression line fits a data set. An *R*-square value of unity indicates a precise fit. Deviation from an *R*-square value of unity indicates decreasing precision.

The results of linear regression of the maximum strength are shown in Fig. 13. It was found that the slopes of linear regression for the three types of concrete vary from 4.67 to 4.24 as concrete strength increases from 60 to 120 MPa. The *R*-square values of linear regression vary from 0.986 to 0.940. This finding was also reported by Jensen,[9] who concluded that the slope becomes smaller as the compressive cylinder strength becomes higher. However, the values of the slope reported here are greater than those reported by Jensen. In Jensen's report,[9] the slopes varied from 4.1 to 2.0 as the concrete strength increased from 25 to 80 MPa. It should be noted that linear regression is an inaccurate estimate, since the relationship between the maximum strength and the confinement is nonlinear for high-strength concrete. When subsets of data with increasing confinement are examined, the apparent slope becomes smaller.

To express the nonlinear relationship between the maximum strength and confinement, a parabolic equation was chosen. The equation can take the form

$$\frac{\sigma_3}{f_c'} = \sqrt{1 + k\left(\frac{\sigma_1}{f_c'}\right)} \qquad (5)$$

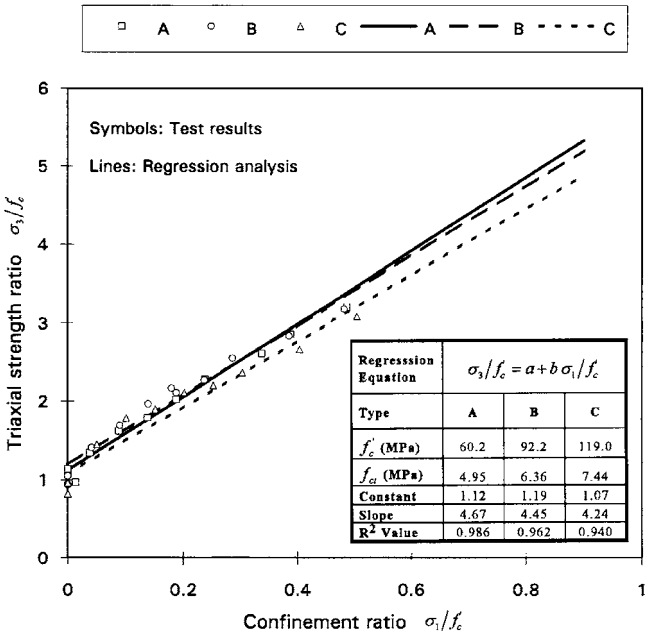


*Fig. 13—Linear regression of maximum strength in triaxial compression.*

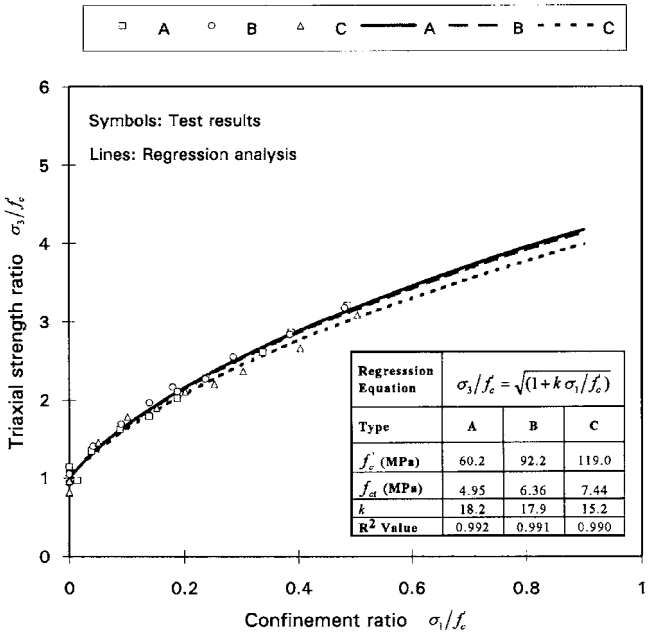


*Fig. 14—Parabolic equation for maximum strength in triaxial compression.*

which automatically passes through the point of uniaxial compression. Here $\sigma_3$ represents the longitudinal compressive peak stress, while $\sigma_1$ represents the confining pressure and $k$ is a constant. The results of regression are shown in Fig. 14 for Types A, B, and C concrete. Obviously, regression using the parabolic equation is a much better representation than the linear regression. The values of Parameter $k$ are also shown in Fig. 14. It was found that the *R*-square values here (0.992 to 0.990) are much closer to unity than those in linear regression.

The parameter $k$ can be related to $f_c'$ through the relation

$$k = 21.2 - 0.05f_c' \quad (6)$$

which gives a very good estimate of $k$ for Types A and C concrete, but slightly underestimates $k$ for Type B concrete. This relation was obtained using regression of the values of $k$ given in Fig. 14. It should be noted that Eq. (5) and (6) are valid only for confinement ratios up to 50 percent.

## CONSTITUTIVE MODELING OF TRIAXIALLY LOADED CONCRETE

Based on Leon's work on the triaxial failure criterion,[14] Pramono and Willam[15] developed a detailed elasto-plastic procedure to model the constitutive behavior of low-strength concrete. An elasto-plastic model requires a description of an initial yield surface that expands to the maximum strength surface in strain hardening and degrades to the residual strength surface in strain softening. In this report, a different model that is modified from the form of Reimann's[16] failure criterion of concrete is suggested. The expressions for the maximum strength surface and residual strength surface are derived, based on the experimental results.

### Maximum strength surface

In the previous section, empirical equations were derived for the maximum strength of concrete under triaxial compression. However, for a constitutive model in a triaxial state of stress, the maximum strength surface must include the cases of uniaxial tension, tension-compression, and tension-tension stress states.

The maximum strength surface in a constitutive model should satisfy the following conditions: 1) passing through the point of uniaxial compression; 2) passing through the point of uniaxial tension; 3) fitting the triaxial compression state; and 4) approaching a hydrostatic state when the confinement is very high.

An expression for the maximum strength surface is suggested using a three-parameter parabolic equation

$$\left(\frac{\sigma_3 - \sigma_1}{f_c'}\right)^2 + a_1\left(\frac{\sigma_3 - \sigma_1}{f_c'}\right) + a_2\left(\frac{\sigma_1}{f_c'}\right) + a_3 = 0 \quad (7)$$

This equation will automatically satisfy the hydrostatic state ($\sigma_1 = \sigma_2 = \sigma_3$) if the confinement ratio $\sigma_1/f_c'$ is very high. There are three parameters involved in the equation that can be used to satisfy the first three conditions discussed previously. Thus, if $a_1$ is determined from regression analysis of the triaxial test results, $a_2$ and $a_3$ can be found by allowing the surface to pass through the points of uniaxial compression and uniaxial tension where the uniaxial tensile strength is assumed to be equal to the splitting tensile strength $f_{ct}$

$$a_2 = \frac{f_{ct}^2 - f_c'^2}{f_c' f_{ct}} + \left(1 - \frac{f_c'}{f_{ct}}\right)a_1 \quad (8)$$

$$a_3 = -1 - a_1 \quad (9)$$

**Table 6—Values of $a_1$, $a_2$, $a_3$, and $a_4$ in the maximum and residual strength equations (Eq. (7) and (11))**

| Type | A | B | C |
|---|---|---|---|
| $f_c'$, MPa | 60.2 | 92.2 | 119.0 |
| $a_1$ | 0.12 | –0.15 | –0.38 |
| $a_2$ | –13.46 | –12.24 | –10.23 |
| $a_3$ | –1.12 | –0.85 | –0.62 |
| $a_4$ | 0.26 | 0.16 | 0.12 |

The values of $a_1$ obtained from regression analyses of the results of three types of concrete are presented in Table 6. We can also derive an approximate equation for $a_1$ as

$$a_1 = 0.63 - 0.0085f_c' \quad (10)$$

The maximum strength surface in the form of Leon's (Romano[14]) failure criterion involved only two parameters that were determined using the uniaxial compressive strength and uniaxial tensile strength. The expression was shown to be satisfactory in Pramono and Willam's[15] model for low-strength concrete. However, as concrete strength increases, both the tension ratio ($f_{ct}/f_c'$) and the confined strength will be reduced. Leon's expression was unable to fit these two conditions simultaneously.

One drawback of Eq. (7) is that the tensile stress is slightly higher than the uniaxial tensile strength in a portion of the range of tension-tension or tension-compression state, depending on the value of $a_1$ . This is also one of the drawbacks in Leon's expression of triaxial strength.

### Residual strength surface

The residual strength surface must pass through the origin of the stress space, since there is no residual level for uniaxial compression. An equation similar to that for the maximum strength surface can be suggested for the residual strength surface

$$\left(\frac{\sigma_3 - \sigma_1}{f_c'}\right)^2 + a_4\left(\frac{\sigma_3 - \sigma_1}{f_c'}\right) + a_2\left(\frac{\sigma_1}{f_c'}\right) = 0 \quad (11)$$

The parameter $a_4$, determined by regression analysis of the test results, is also included in Table 6.

The suggested maximum strength surface and the residual surface are plotted in Fig. 15 and 16 for Type A and C concrete, together with the test results. These two surfaces become asymptotic at high confinement ratios.

## CONCLUSIONS

In this report, the results of experimental work on the mechanical properties of high-strength concrete were presented. The tests included the compressive cylinder test, splitting test, notched-beam test, and triaxial compression test for concretes having strengths of 60, 90, and 120 MPa. It was concluded that although the tensile strength and fracture energy increase with an increase in compressive strength, high-strength concrete is less ductile than normal concrete in both tension and compression. It was also concluded that confinement of the concrete will increase the maximum and

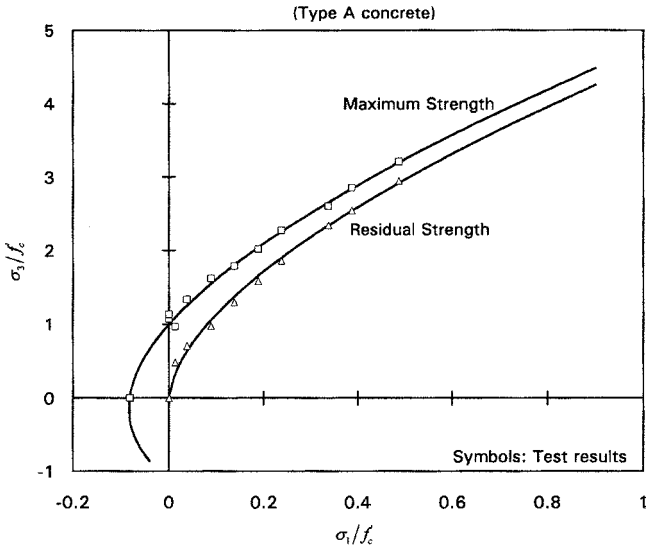


*Fig. 15—Maximum and residual strength surfaces (Type A concrete).*

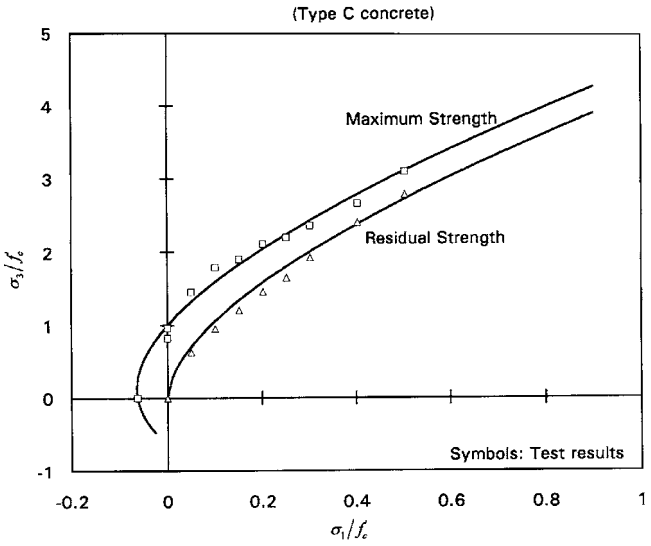


*Fig. 16—Maximum and residual strength surfaces (Type C concrete).*

residual compressive strengths significantly and also improve the ductility of concrete. The test results have been used to establish expressions of maximum and residual strengths in a finite element constitutive model for high-strength concrete. It is recommended that further tests by independent researchers be carried out on concrete in this range of strength to confirm our results.

## ACKNOWLEDGMENTS

The work described in this paper was carried out as part of the research program of the Canadian Network of Centers of Excellence on High-Performance Concrete. Funding was provided by the NCE program. The authors acknowledge Dr. S. Alexander for his assistance in the design and conduct of the tests. The testing was carried out in the I. F. Morrison Structural Engineering Laboratory of the University of Alberta, Edmonton, Canada.

## NOTATION

$a_1,...a_4$ = constants in suggested constitutive model
$b$ = width of notched beam
$d$ = height of notched beam
$D$ = diameter of cylinder specimen
$f'_c$ = compressive cylinder strength
$f_{ct}$ = split-cylinder strength
$G_{cr}$ = tensile fracture energy
$h$ = height of notch
$H$ = height of cylinder specimen
$k$ = constant in empirical parabolic equation for triaxial compressive strength
$L$ = length of splitting cylinder and notched beam
$mg$ = weight of notched beam
$P$ = load acting on specimen
$\delta$ = load-point displacement of notched beam
$\delta_{max}$ = rupture displacement of notched beam when load drops to zero
$\sigma_1$ = confining stress on triaxially loaded cylinder (positive for compression)
$\sigma_3$ = longitudinal stress on triaxially loaded cylinder (positive for compression)

## CONVERSION FACTORS

1 mm = 0.039 in.
1 MPa = 145 psi

## REFERENCES

1. *CEB/FIP Report*, "High Strength Concrete—State of the Art Report," *SR90/1, Bulletin d'Information* No. 197, Aug. 1990.

2. Reinhart, H. W., "Fracture Mechanics of an Elastic Softening Material Like Concrete," *Heron* (The Netherlands), V. 29, No. 2, 1984, p. 42.

3. Gopalaratnam, V. S., and Shah, S. P., "Softening Response of Concrete in Direct Tension," *Technological Institute Report*, Northwestern University, Evanston, 1984.

4. Willam, K.; Hurlbut, B.; and Sture, S., "Experimental and Constitutive Aspects of Concrete Failure," *Proceedings, U.S.-Japan Seminar on Finite Element Analysis of Reinforced Concrete Structures*, Tokyo, 1985, ASCE, Special Publication, New York, pp. 226-254.

5. Hillerborg, A., "Theoretical Basis of a Method to Determine the Fracture Energy $G_F$ of Concrete," *RILEM Technical Committee 50*, 1985.

6. Peterson, P. E., "Fracture Energy of Concrete: Method of Determination," *Cement and Concrete Research*, V. 10, pp. 77-89.

7. Richart, F. E.; Brandtzaeg, A.; and Brown, R. L., "Study of the Failure of Concrete under Combined Compressive Stresses," *Bulletin* 185, University of Illinois Engineering Station, Urbana, Nov. 1928, pp. 104.

8. Palaniswamy, R., and Shah, S. P., "Fracture and Stress-Strain Relationship of Concrete under Triaxial Compression," *Journal of the Structural Division*, ASCE, V. 100, No. ST5, May 1974, pp. 901-916.

9. Jensen, J. J., and Bjerkeli, L., "Effect of Water Pressure on Concrete Structures," *Water Absorption, Static Strength and Strain Development Tests, SINTEF Report*, STF65, F87037.

10. Carrasquillo, R. L.; Nilson, A. H.; and Slate, F. D., "Properties of High Strength Concrete Subject to Short-Term Loading," ACI JOURNAL, *Proceedings* V. 78. No. 3, May-June 1981, pp. 171-178.

11. Hillerborg, A., "Numerical Methods to Simulate Softening and Fracture of Concrete," *Fracture Mechanics of Concrete: Structural Application and Numerical Calculation*, Sih, C. C.; Tomaso, D.; and Kluwer, A., eds., Academic Publishers, pp. 141-170.

12. RILEM Technical Committee 50, "Determination of the Fracture Energy of Mortar and Concrete by Means of Three-Point Load Tests on Notched Beams," *RILEM Draft Recommendation, Materiaux et Constructions*, V. 18, No. 106, 1985, pp. 285-290.

13. Hurlbut, B. J., "Experimental and Computational Investigation of Strain-Softening in Concrete," MS thesis, University of Colorado, Boulder, 1985.

14. Romano, M., "On Leon's Criterion," *Meccanica*, Mar. 1969, pp. 48-66.

15. Pramono, E., and Willam, K., "Fracture Energy-Based Plasticity Formulation of Plain Concrete," *Journal of Engineering Mechanics*, V. 115, No. 6, ASCE, 1989, pp. 1183-1204.

16. Reimann, H., "Kritische Spannungszustande der Betons bei mehrachsiger, ruhender Kurzzeit-belastung," *Deutscher Ausschuss fur Stahlbeton* (Berlin), V. 175, 1965.